Journal of Solar Energy Research (JSER)

Journal homepage: www.jser.ut.ac.ir

Comparative Thermal Analysis of Conventional and Square-Corrugated Basin Solar Stills in Basra

Esraa Hassanain Yousif[a,*], Adnan Abdullah Ateeq[b], and Tahseen Ali Jabbar[a]

[a]*Thermal Mechanical Engineering Department, Engineering Technical College, Southern Technical University, Basrah, Iraq*

[b]*Chemical and Petrochemical Engineering Department, Engineering Technical College, Southern Technical University, Basrah, Iraq*

ARTICLE INFO

Article Type:

Research Article

Received:2026.05.17
Accepted in revised form:2026.07.29

Keywords:
Solar still; Basin geometry; Square-corrugated basin; Thermal performance; Freshwater productivity; CFD

A B S T R A C T

Solar stills represent a promising technology for decentralized freshwater production in arid and semi-arid regions. Nevertheless, their large-scale utilization remains limited by their relatively low distillate productivity and thermal efficiency. To address this limitation, the present study numerically investigates the influence of basin geometry on the thermal performance and productivity of a single-slope solar still. The analysis compares a conventional flat basin with a square-corrugated basin under identical operating conditions in Basra, Iraq, on 28 October 2025. A transient two-dimensional CFD model was developed in ANSYS Fluent, and the predicted basin water and glass cover temperatures were coupled with Dunkle correlations to estimate the hourly and daily distillate yield. The square-corrugated basin showed a clear improvement over the flat basin, with peak hourly productivity increasing from 0.72 to 0.89 kg/m²·h and cumulative daily yield increasing from 2.97 to 3.9 kg/m²·day. The average daily thermal efficiency also improved from 44.7% to 67.3%. Overall, this geometric modification achieved a 31.12% improvement in freshwater production. These results indicate that increasing the effective heat-transfer area by modifying the basin geometry improved the thermal behavior of the solar still and significantly enhanced its productivity under identical climatic conditions.

*Corresponding Author Email:esraa.h.yousif@fgs.stu.edu.iq

Cite this article: Yousif,E Hassanain, Ateeq,A Abdullah and Jabbar,T Ali. (2026). Comparative Thermal Analysis of Conventional and Square-Corrugated Basin Solar Stills in Basra. Journal of Solar Energy Research, 11(3), 3182-3195. doi: 10.22059/jser.2026.414590.1741

DOI: 10.22059/jser.2026.414590.1741

1. Introduction

Solar energy is widely recognized as a clean, renewable, and environmentally friendly energy source that produces no harmful emissions during operation. Its growing adoption has been driven by concerns over global warming, fossil fuel depletion, and environmental degradation. Consequently, solar energy has become increasingly important in both photovoltaic and solar thermal technologies, particularly because of the wide applicability of solar thermal systems in engineering and energy-related fields [1] .

Solar desalination is a sustainable method for producing freshwater from saline water using solar energy, and it can also be applied to brackish water and some industrial effluents. Among desalination technologies, solar stills are regarded as one of the most economical and environmentally friendly options because of their simple construction, low cost, and ease of operation. However, their practical application remains limited by low freshwater productivity, which has made performance enhancement a major focus of current research [2].

Consequently, solar stills have attracted significant research interest worldwide. Various design configurations have been developed to improve water yield, including tubular, pyramidal, spherical, hemispherical, triangular, inclined, stepped, cascade, wick-type, double-basin, and double-slope solar stills. In addition, numerous enhancement methods have been explored, such as phase change materials, glass-cover cooling, internal and external reflectors, sun-tracking systems, wick materials, baffle-suspended absorber plates, vacuum techniques, floating porous absorbers, energy-storage materials, evacuated tubular collectors, and external condensers [3] [4] [5] .

The influence of corrugated absorber plates on solar still performance has been examined in several studies. In general, increasing basin surface complexity enhances evaporation by enlarging the effective heat-transfer area and strengthening thermal interaction between basin water and the absorber surface. However, the investigated designs, enhancement techniques, and reported performance gains vary considerably. Furthermore, relatively few studies have specifically addressed the integration of corrugated plates into conventional solar still configurations. Several studies have investigated the influence of corrugated absorber geometries on solar still performance and reported noticeable improvements in freshwater productivity. Omara et al. [6] experimentally investigated a single-slope solar still equipped with a corrugated absorber, wick, and reflectors. Their results showed that the corrugated absorber improved daily freshwater productivity by 55.36% compared with a flat-basin still. However, the study combined corrugation with other enhancement techniques, making it difficult to isolate the individual effect of basin corrugation. Ghandourah et al. [7] examined the performance of a pyramid solar still integrated with a corrugated absorber plate. The study reported a 52.54% increase in daily productivity compared with a conventional configuration. Nevertheless, the work mainly focused on experimental productivity and economic analysis, with limited discussion of the internal CFD-based heat-transfer mechanisms. Sharshir et al. [8] investigated a pyramid solar distiller using nanofluid integrated with a V-corrugated absorber and wick material. Their results indicated that the V-corrugated surface enhanced productivity by 28.38%. However, because several enhancement techniques were applied simultaneously, the independent influence of the corrugated geometry was not fully isolated. Likewise, Kabeel [9] studied experimentally the effect of absorber corrugation shape on the performance of a hemispherical solar still. The study reported that the square-corrugated absorber improved daily productivity by 27.08% compared with the flat absorber. Corrugated absorbers have also been applied in tubular and other modified solar still configurations. A. E. Kabeel [10] reported that the use of a V-corrugated wick absorber in a tubular solar still increased freshwater yield and efficiency by 44.82% and 46.86%, respectively. Similarly, Prasada [11] found that maintaining an optimum water depth of 5 mm in a corrugated tubular solar still increased productivity by 70.45%. Elshamy [12] showed that replacing a flat absorber with a semi-circular corrugated absorber increased productivity from 19.33 to 26.47%, while Abdelaziz [13] reported that incorporating a corrugated aluminium basin into a tubular solar still improved productivity by approximately 21.4%. Several researchers further combined corrugated basins with additional enhancement techniques. Hafs [14] reported a productivity improvement of 109% when corrugation was combined with thermal energy storage material, while integration with a parabolic trough collector increased productivity by more than 549%. Zeid [15] reported a 22.39% increase in productivity by combining a V-corrugated basin with mirrors, a flat-plate collector, and nanofluids. Shalaby [16] found an additional 12% improvement when phase change materials were added to a V-corrugated basin. Jodah

[17] reported a 44% increase in daily productivity using a corrugated circular basin with rear solar tracking, while Kabeel [18] obtained a 68.82% increase by combining a V-corrugated basin with a reversed solar collector. In addition, Essa [19] found that a triangular corrugated absorber in a pyramidal solar still improved productivity by approximately 61%, with an energy efficiency of 44.2%, whereas Sharshir [20] reported a more moderate increase of 11% with a simple corrugated basin in a hemispherical solar still. Recent studies have explored alternative approaches for enhancing solar still performance. Dumka et al. [21] investigated the integration of a solar fountain into a conventional solar still and reported a performance improvement of approximately 35% compared with the conventional design. Similarly, Kumar et al. [22] evaluated a conventional solar still augmented with a peat–perlite blend and demonstrated enhanced thermal performance and freshwater productivity by 79.65%, thermal and energy efficiencies by 49.93% and 73.34%, respectively. Dumka et al. [23] employed gel balls as a thermal enhancement medium and achieved increases of approximately 36.14% in freshwater productivity and 31.6% in thermal efficiency. Furthermore, Dumka et al. [24] investigated wax-infused glass as a latent thermal-storage medium and reported sustained freshwater production during low-radiation periods. Productivity improved by 17%. Likewise, Dumka et al. [25] utilized saltwater bottles as a low-cost thermal-storage technique and observed improvements in daily distillate yield and efficiency by 25.4% and 25%, respectively, compared with a conventional solar still. More recently, Chauhan et al. [26] developed a Levenberg–Marquardt artificial neural network model for predicting the performance of conventional and modified solar stills and achieved high prediction accuracy under different operating conditions.

Overall, previous studies have demonstrated that corrugated and modified basin geometries can effectively enhance solar still productivity. However, the direct thermal contribution of square-corrugated basins remains insufficiently investigated, particularly through detailed CFD analysis under identical operating conditions. Therefore, the present study develops a two-dimensional CFD model to investigate a solar still equipped with a square-corrugated basin under the climatic conditions of Basra, Iraq. The square-corrugated geometry was selected because it increases the effective heat-transfer area while maintaining geometric simplicity. Unlike previous studies, the effect of basin geometry was isolated by maintaining identical projected basin area and basin water mass in both the conventional and modified configurations. In addition to freshwater productivity, the study evaluates temperature distribution, convective and evaporative heat-transfer coefficients, and thermal efficiency, providing a clearer physical interpretation of the heat-transfer mechanisms responsible for performance enhancement.

2. Methodology

The square-corrugated basin was selected because it increased the effective heat-transfer area while maintaining geometric simplicity. Although other corrugation profiles, such as V-shaped, triangular, sinusoidal, and trapezoidal geometries, have been reported in the literature, the present study focuses on the square-corrugated configuration to isolate its thermal effect under identical operating conditions.
This study employs an integrated methodology that combines measured climatic data with computational fluid dynamics (CFD) simulations to evaluate the thermal and productivity performance of conventional and square-corrugated basin solar stills under the climatic conditions of Basra, Iraq. To ensure a fair comparison, both configurations were designed with the same projected basin area and basin water mass.

The overall methodology is illustrated in Fig. 1. Initially, hourly climatic data, including solar irradiance and ambient temperature, were collected and used as time-dependent inputs for the numerical model. Subsequently, the solar still geometries were developed and discretized using computational meshes. The governing equations and physical assumptions were then implemented in ANSYS Fluent, together with the corresponding boundary and initial conditions. After obtaining the numerical solution, convergence and validation procedures were performed to ensure the reliability of the CFD predictions. Finally, the simulation results were post-processed, and Dunkle’s correlations were applied to calculate the heat-transfer coefficients, freshwater productivity, and thermal efficiency. The details of each stage are presented in the following sections.

2.1 Site Location and Climatic Conditions

On-site measurements were performed in Basra, Iraq, on 28 October 2025. Solar irradiance and ambient temperature data were recorded between 07:00 and 16:00 and then implemented as time-dependent boundary conditions in the computational simulations to represent realistic climatic conditions. Solar radiation intensity was measured with a TES 1333R solar irradiance meter, and ambient air temperature was monitored with a calibrated precision thermometer.

The measured climatic data employed in the numerical simulations are presented in Table 1. Since the glass cover of the solar still is inclined, the measured solar irradiance was corrected using the cosine law to determine the effective irradiance incident on the inclined surface. The corrected irradiance values were then applied as the solar radiation input in the CFD model. Wind velocity was

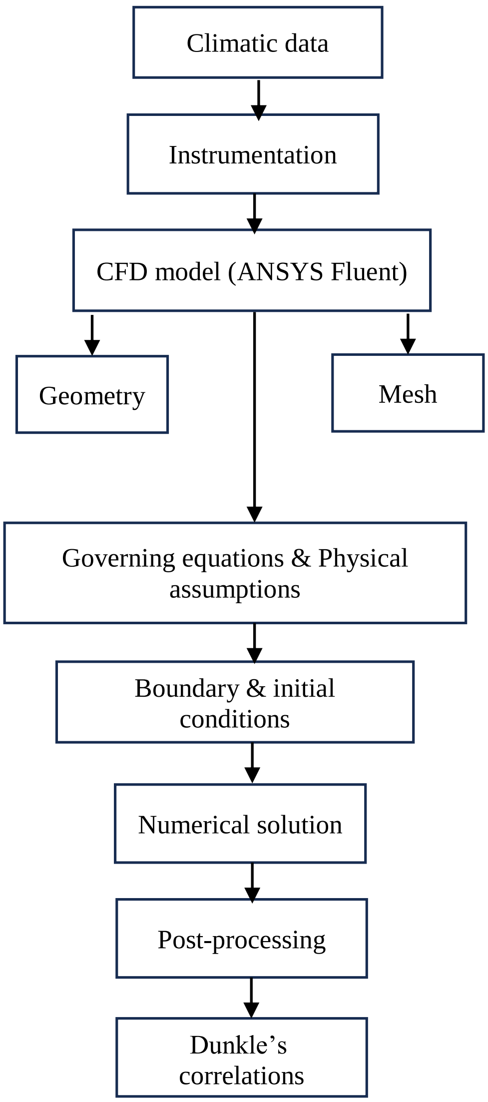

Figure 1. shows the methodological flow diagram

not introduced as a time-dependent boundary condition; instead, its influence was represented through the external convective heat-transfer boundary condition imposed on the exposed surfaces. This approach was adopted to ensure that the numerical comparison remained focused on the effect of basin geometry under identical climatic conditions.

Table 1. Hourly climatic input data used for the Basra simulation case

Time	Ambient temperature, Ta (°C)	Measured solar irradiance, I (W/m²)	Inclination-corrected irradiance, Iθ (W/m²)
7:00 AM	23.41	279.29	241.86
8:00 AM	26.36	468.11	405.39
9:00 AM	28.44	614.69	532.32
10:00 AM	31.37	711.66	616.30
11:00 AM	33.91	793.40	687.08
12:00 PM	34.56	809.87	701.35
1:00 PM	35.86	615.47	533.00
2:00 PM	35.57	390.21	337.93
3:00 PM	35.10	239.77	207.64
4:00 PM	32.87	37.40	32.39

The measured data indicate that the ambient temperature increased from 23.41°C in the morning to a maximum of 35.86°C at 1:00 PM, while the corrected solar irradiance reached a peak value of 701.35 W/m² at 12:00 PM.

2.2 Numerical Model

A numerical model was developed in ANSYS Fluent 19 to simulate both the conventional flat basin and the square-corrugated basin configurations. Dunkle's model was selected in place of the VOF model due to its lower computational cost and acceptable prediction accuracy. The model incorporates heat conduction, natural convection, and radiative heat transfer, whereas the distillate productivity is calculated using Dunkle-type correlations derived from the temperature fields obtained from the CFD analysis.

2.2.1 Geometry Design

A two-dimensional (2D) geometric model of the single-slope solar still was established in ANSYS Design Modeler. The model domain comprised the absorber basin, water layer, glass cover, side walls, and the wooden insulation layer located beneath the basin, with all material layers explicitly included. Two basin geometries were investigated while maintaining the same projected basin area (0.016 m²) and water mass: a conventional flat basin and a square-corrugated basin. For both configurations, the basin length was fixed at 1000 mm, whereas the right and left wall heights were 470 mm and 190 mm, respectively. The key geometric dimensions and material properties adopted in the numerical simulations are summarized in Table 2.

Table 2. Geometrical parameters of conventional and square-corrugated basins

Parameters	Conventional Basin	Square-Corrugated Basin
Basin Area(m^2)	0.016	0.016
Basin Length(mm)	1000	1000
Basin Height(mm)	16	17.4
Right / Left Side Height(mm)	470/190	470/190
Pitch of corrugation (p_h)(mm)	-	10
Height of corrugation, (h)(mm)	-	2.8
Number of corrugations	-	50
Basin / Side-wall Material	Aluminum	
Glass/ Insulation Material	Glass / Wood	

For the conventional basin, the effective evaporative area equals the horizontal projected area of the water surface, that is, 0.016 m². In contrast, the square-corrugated basin incorporates a periodic corrugation characterized by a pitch (p_h) and corrugation height (h), which improves heat transfer and increases the surface area at the water–air interface. The effective surface area associated with a single square corrugation, A_{square}, is evaluated as:

$$A_{square} = 2p_h + 2h \quad (1)$$

where:

• p_h: the horizontal pitch of the corrugation.

• h : the vertical height (depth) of the corrugation.

The total effective area of the corrugated basin, A_{total}, is obtained by multiplying A_{square} by the number of corrugations *N*:

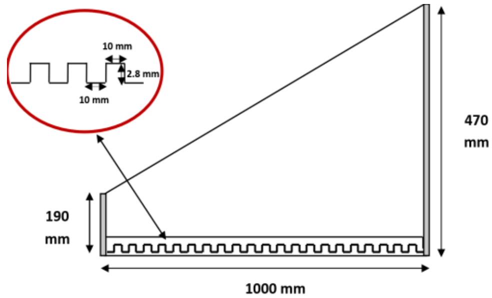

Figure 2. Geometry of the square corrugated basin in the solar still

$$A_{total} = N \times A_{square} \quad (2)$$

The two equations above were derived from the geometric analysis of the corrugation shape. Using the adopted geometric parameters (Table 2), the square-corrugated basin attains a significantly larger effective evaporative area than the conventional basin. The schematic representation of the square-corrugated basin geometry is shown in Fig 2.

2.2.2 Mesh Generation

The computational mesh was developed in ANSYS Meshing using an unstructured, quadrilateral-dominant topology to accommodate the geometric features of both basin configurations. A uniform characteristic element size of 0.004 m was employed throughout the computational domain to balance numerical accuracy and computational efficiency, and no local refinement was introduced in the baseline mesh. The final meshes contained 22,457 cells for the conventional basin and 22,972 cells for the square-corrugated basin, with similar node distributions. Further details of the mesh are provided in Table 3 and Fig 3.

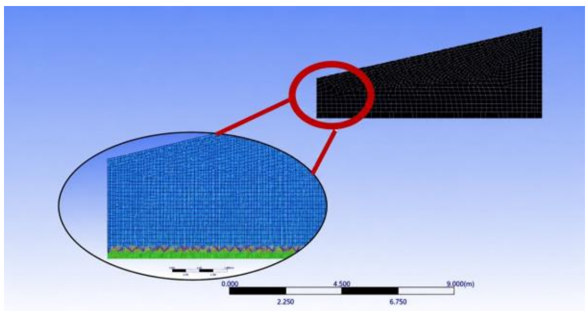

Figure 3. Computational mesh of the model

Table 3. Mesh characteristics for the conventional and square-corrugated basins

Parameters	Conventional Basin	Square Corrugated Basin
Nodes	22881	23255
Elements	22457	22972
Mesh Size (m)	0.004	0.004
Mesh Type	Quadrilateral Dominant	

A mesh independence test was performed by varying the global element size and examining its effect on the predicted hourly freshwater productivity of the square-corrugated basin. Within the mesh-size range of 0.004–0.009 m, the numerically predicted peak hourly yield changed only from 0.009729 to 0.011958 kg/m²·h, which indicates that additional mesh refinement produces only minor variations in the key performance parameter relative to the corresponding increase in computational cost. Accordingly, the mesh with a characteristic element size of 0.004 m was adopted in all subsequent simulations. The influence of mesh size on the predicted hourly productivity is illustrated in Fig. 4.

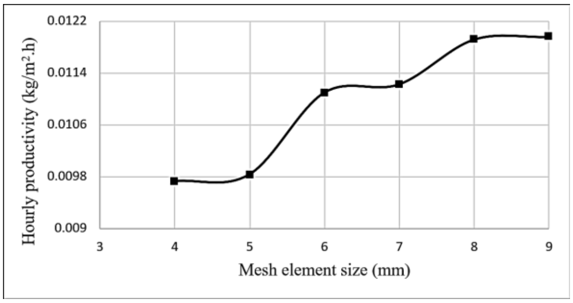

Figure 4. Mesh independence study based on mesh element size

2.2.3 Governing Equations and Physical Assumptions

The fluid flow and heat transfer within the solar still are described by the conservation equations of mass, momentum, and energy [27]:

2.2.3.1 Governing Equations

The Continuity Equation is expressed as [27]:

$$\frac{\partial \rho}{\partial t} + \text{div}(\rho u) = S_m \quad (3)$$

The Momentum Conservation Equation is expressed as [27]:

$$\frac{\partial}{\partial t}(\rho u) + \nabla.(\rho u u) = -\nabla p + \nabla.(\bar{\bar{\tau}}) + \rho g + \vec{F} \quad (4)$$

The Energy Conservation Equation is expressed as [27]:

$$\frac{\partial}{\partial t}(\rho E) + \nabla.\left(u(\rho E + p)\right) = \nabla.\left(K_{eff}\nabla T - \sum_j h_j \vec{J}_j + (\bar{\bar{\tau}}.u)\right) + S_h \quad (5)$$

2.2.3.2 Physical Assumptions

To simplify the numerical analysis while keeping the physical behaviour of the system reasonable, the following assumptions were considered:

- The flow inside the solar still is assumed to be turbulent and is represented using the k–ε turbulence model.
- The Discrete Ordinates (DO) model was used to replicate the radiation within the solar still, particularly for materials such as glass and water that have limited transparency.
- Air inside the solar still was modeled using the Boussinesq approximation.
- The thermophysical properties of air and water were taken as constant.
- The freshwater productivity was calculated separately using Dunkle's correlations based on the temperature results obtained from the numerical simulations.

2.2.4 Boundary and Initial Conditions

To replicate actual working conditions, the glass cover is exposed to a combined convective-radiative boundary and time-dependent solar irradiance, and is treated as partially transparent. The outer lateral surfaces and layer beneath the basin are assumed to be thermally insulated. An initial temperature of 23 °C is imposed across the entire domain. Results demonstrate that the convective coefficients considerably influence peak water temperature, as outlined in Table 4.

Table 4. Boundary conditions and thermal radiative properties applied to different components of the solar still

Parameters	Applied boundary conditions
Glass	Combined convection and radiation heat transfer and Semi-transparent (Diffuse Fraction=1)
Wall	Adiabatic insulation (heat flux= 0 w/m^2) and opaque (Diffuse Fraction=1)
Wood	Convection heat transfer and Opaque (Diffuse Fraction=1)

2.2.5 Numerical Model Verification

The governing equations were solved in ANSYS Fluent using the finite volume method. Pressure–velocity coupling was achieved through the coupled algorithm. A second-order discretization scheme was employed for the pressure and momentum equations, whereas first-order upwind schemes were used for the energy and turbulence equations. All simulations were performed in transient mode.

To ensure numerical accuracy and stability, convergence was monitored using both residual histories and the average basin-water temperature. The solution was considered converged when the residuals of continuity and velocity fell below 10^{-3}, while those of the energy equation and DO radiation intensity were reduced below 10^{-6}.

The residual convergence history is presented in Fig. 5. As shown, the residuals of continuity and velocity decreased to values below 10^{-3}, whereas the residuals of the energy equation and DO radiation intensity converged to values lower than 10^{-6}. In addition, the monitored average water temperature exhibited stable behavior throughout the simulation. These results confirm the numerical stability and convergence of the adopted CFD solution procedure.

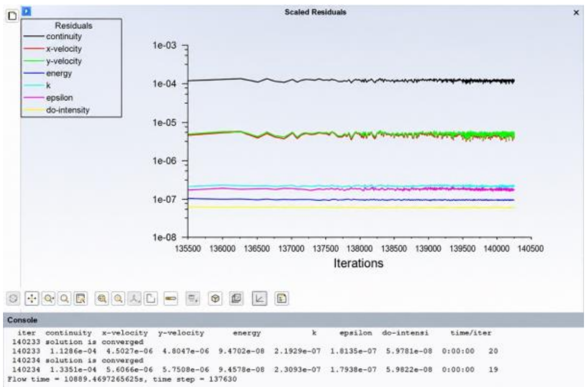

Figure 5. Residual convergence history of the CFD simulation in ANSYS Fluent

2.2.6 Post-Processing of Results

Following each simulation, the predicted basin-water temperature (T_w) and glass-cover temperature (T_g) were substituted into Dunkle's correlations to determine the heat-transfer coefficients, evaporative heat flux, and distillate yield. The thermal efficiency and enhancement ratio were then evaluated to quantify the performance gain achieved by the square-corrugated basin in comparison with the conventional basin.

The hourly distillate yield (m_{ew}) was computed based on Dunkle's model [28] as follows:

$$\dot{m}_{ew} = \frac{\dot{q}_{ew}}{h_{fg}} = \frac{h_{ew}(T_w\text{-}T_g)}{h_{fg}} \quad (6)$$

where the evaporative heat transfer coefficient (h_{ew}) [28] and the latent heat of vaporization (h_{fg}) are determined by [10]:

$$h_{ew} = 16.273 \times 10^{-3} \times h_{cw} \times \frac{(P_w\text{-}P_g)}{(T_w\text{-}T_g)} \quad (7)$$

$$h_{fg} = 10^3[\,2501.9\text{-}2.40706\,T_w + 1.192217 \times 10^{-3}T_w^2\text{-}1.5863 \times 10^{-5}T_w^3] \quad (8)$$

where the temperatures T_w and T_g are measured in degrees Celsius (°C), the heat transfer coefficients h_{ew} and h_{cw} are expressed in (W/m² · K), the latent heat of evaporation h_{fg} is expressed in (J/kg), and the hourly productivity m_{ew} is expressed in (kg/m²·h). The hourly efficiency (η_h) and enhancement ratio (ER) were determined by [28] :

$$\eta_h = \frac{m_{ew} \times h_{fg}}{I \times A_s \times 3600} \quad (9)$$

$$ER(\%) = \frac{x_{mod}\text{-}x_{ref}}{x_{ref}} \times 100 \quad (10)$$

where ER is the enhancement ratio (%); x_{mod} is the value of the parameter for the modified (corrugated) basin; x_{ref} is the value of the parameter for the conventional basin.

2.2.7 Validation of Results with Previous Study

The developed numerical framework was validated by comparison with the experimental results reported by Dwivedi and Tiwari [29], which was selected because it provides published hourly distillate-yield data for a solar still configuration suitable for evaluating the predictive capability of the present model. The hourly distillate yield was adopted as the main validation parameter because it reflects the combined influence of heat absorption, water heating, evaporation, and condensation processes.

For the validation simulation, ANSYS Fluent was employed using the energy equation, radiation model, and k–ε turbulence model. Convective boundary conditions were specified for the glass cover and walls, while a heat-flux condition was imposed at the basin surface. A time step of 60 s was adopted, and solution convergence was achieved when the residuals decreased below 10^{-4}. The hourly distillate yield was calculated using Dunkle's correlations.

The comparison showed good agreement between the numerical and experimental results. The numerical model predicted a peak hourly productivity of 2.42 kg/m²·h, compared with the experimental value of 2.35 kg/m²·h. The validation also yielded an RMSE of 0.4300 and a correlation coefficient of 0.948441, indicating that the model was able to reproduce the experimental productivity trend with acceptable accuracy. The slight differences between the numerical and experimental values may be attributed to variations in operating conditions, simplifications in the numerical assumptions, and the empirical nature of the heat-transfer correlations. Therefore, the validation results, illustrated in Fig. 6, support the adequacy and reliability of the present numerical approach for predicting the thermal performance and productivity of the investigated solar still configurations.

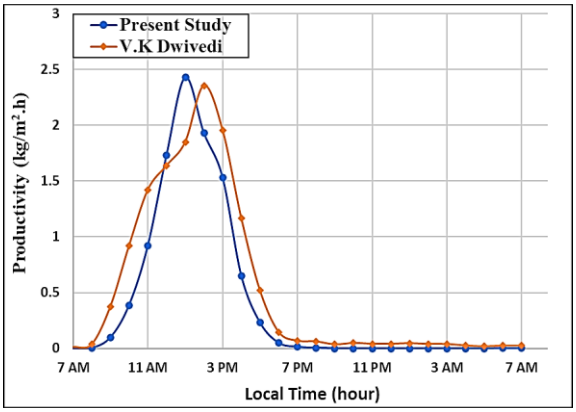

Figure 6. Comparison of Hourly Productivity between the Present Study and the Previous Study

2.2.8 Uncertainty and Error Estimation

An uncertainty analysis was conducted to assess the reliability of the calculated productivity and thermal efficiency. The main sources of uncertainty were associated with the measured climatic inputs (solar irradiance and ambient temperature), the CFD-predicted basin-water and glass-cover temperatures, and the empirical correlations used to estimate heat and mass transfer. Numerical uncertainties were minimized through mesh-independence verification and convergence monitoring. Therefore, the reported results should be interpreted within the combined influence of measurement accuracy, numerical discretization, and post-processing calculations. The main sources of uncertainty considered in the present study are summarized in Table 5.

Table 5. Main sources of uncertainty considered in the present study

Source	Source of uncertainty
Solar irradiance meter	TES 1333R accuracy (± 0.5%)
Thermometer	Thermometer accuracy (±1°C)
Mesh resolution	Mesh independence test
Numerical convergence	Residual criteria
Dunkle correlations	Empirical correlation uncertainty

3. Results and Discussion

3.1 Simulation Results

Figure 7 compares the temperature fields of the conventional and square-corrugated basins, shown in Figs. 7a–7c and Figs. 7d–7f, respectively. The internal temperature field of the solar still follows the diurnal variation of solar irradiance. At 09:00 AM, solar radiation initiates a gradual rise in basin-water temperature, while weak natural convection begins to develop inside the enclosure in both configurations (Fig. 7a and Fig. 7d). At 12:00 PM, the temperature field becomes more strongly stratified, with a clear thermal gradient extending from the heated basin toward the glass cover (Fig. 7b and Fig. 7e). At this stage, the square-corrugated basin consistently exhibits higher water temperatures than the conventional basin due to its enlarged effective heat-transfer area. By 3:00 PM, although solar irradiance declines, elevated temperatures persist in both configurations, especially in the corrugated basin, as a result of thermal inertia (Fig. 7c and Fig. 7f). This delayed cooling prolongs the temperature difference between the basin water and the glass cover and thus maintains the driving potential for evaporation and condensation during the late afternoon period.

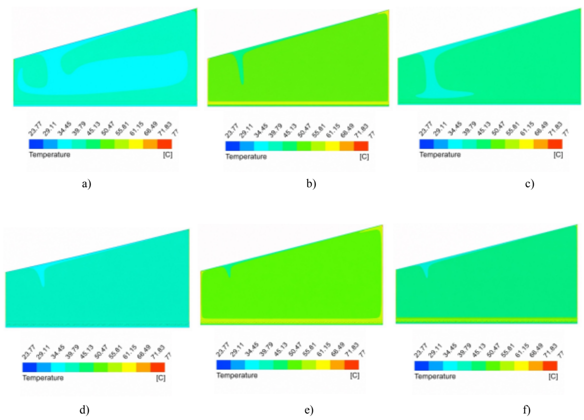

Figure 7. The temperature contours for both the conventional and corrugated basins are presented at the same time intervals: 9:00 AM, 12:00 PM, and 2:00 PM

3.2 Analytical Results

A comparative analysis was conducted between the conventional flat basin and the square-corrugated basin while maintaining identical projected basin area and basin-water mass. The thermal and productivity characteristics of both configurations were evaluated using Dunkle-based post-processing of the CFD-predicted temperature fields.

Figure 8 presents the hourly variation of solar irradiance and ambient temperature on 28 October 2025. The solar irradiance increased progressively during the morning period, reaching a maximum corrected value of 701.35 W/m² at noon before gradually decreasing during the afternoon. In contrast, the ambient temperature continued to increase after noon and attained its peak value of 35.86 °C at 1:00 PM. This temporal lag between maximum solar irradiance and ambient temperature is attributed to the thermal inertia of the surrounding environment.

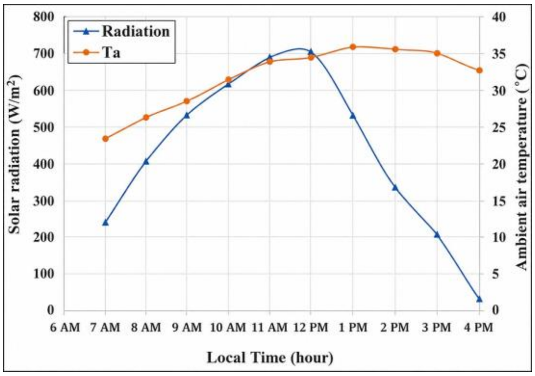

Figure 8. Hourly variation of solar radiation and ambient air temperature during the experimental day

Figures 9 and 10 compare the basin-water and glass-cover temperatures for the conventional and square-corrugated basin solar stills. Throughout the operating period, the square-corrugated basin maintained higher basin-water temperatures than the conventional configuration, with a maximum temperature difference of approximately 2.72 °C at noon. This improvement is primarily attributed to the increased effective heat-transfer area provided by the corrugated geometry, which enhances heat absorption and promotes a more uniform thermal distribution within the basin. Similarly, the glass-cover temperature of the square-corrugated basin remained slightly higher than that of the conventional basin, with a maximum difference of approximately 0.35 °C at 1:00. Consequently, a larger temperature difference was sustained between the basin water and the glass cover, thereby strengthening the evaporation–condensation cycle and enhancing freshwater production.

Figures 11 and 12 illustrate the variations in the convective and evaporative heat-transfer coefficients for both configurations. The square-corrugated basin exhibited consistently higher values of both coefficients throughout the operating period. This behavior is primarily attributed to the increase in the effective heat-transfer area resulting from the corrugated geometry, which enhances energy absorption and promotes more efficient heat transfer from the basin surface to the water layer. Consequently, the basin water attains higher temperatures, leading to an increase in the temperature difference between the basin water and the glass cover. According to Dunkle's formulation, both the convective and evaporative heat-transfer coefficients are strongly influenced by the temperature and vapor-pressure differences between the evaporating water surface and the condensing glass cover. Therefore, the higher basin-water temperatures achieved by the square-corrugated basin intensify the evaporation process and increase the rate of vapor transport within the enclosure. As a result, the convective heat-transfer coefficient increases due to enhanced heat exchange between the humid air and the glass cover, while the evaporative heat-transfer coefficient increases because of the greater vapor-pressure. These combined effects indicate that the square-corrugated geometry improves not only heat absorption but also the overall heat- and mass-transfer processes governing freshwater production.

Figure 13 presents the hourly freshwater productivity of the conventional and square-corrugated basin solar stills. In both configurations, productivity follows the general trend of solar irradiance and basin-water temperature, increasing during the morning period and reaching its maximum value around noon. However, the square-corrugated basin consistently produces higher freshwater yield throughout the day due to the enhanced thermal conditions established inside the still. The higher basin-water temperature increases the saturation vapor pressure at the water surface, thereby accelerating evaporation. Simultaneously, the maintained temperature difference between the basin water and the glass cover sustains condensation, resulting in a greater distillate yield. Consequently, the peak hourly productivity increased from 0.72 kg/m²·h for the conventional basin to 0.89 kg/m²·h for the square-corrugated basin.

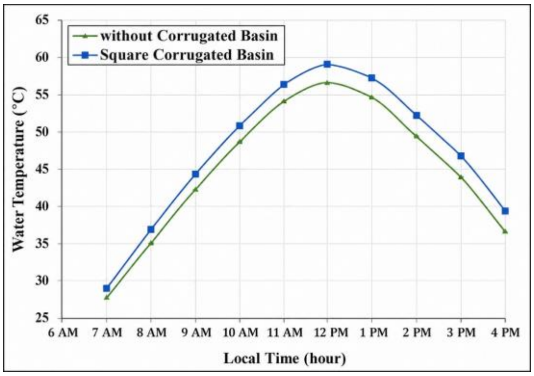

Figure 9. Comparison of water temperature between the conventional basin and the square corrugated basin solar still

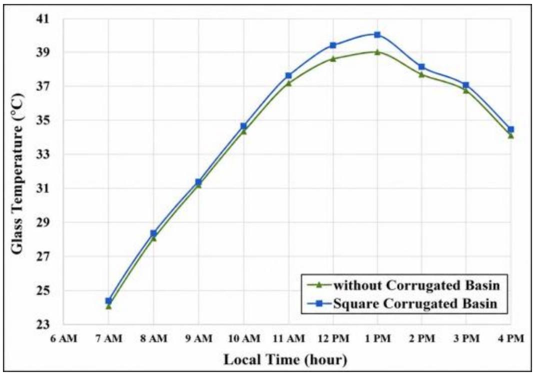

Figure 10. Comparison of glass cover temperature between the conventional basin and the square corrugated basin solar still

Figure 14 shows the cumulative freshwater productivity of both configurations. The difference between the two curves increases progressively with operating time, indicating that the productivity advantage of the square-corrugated basin is maintained throughout the day rather than occurring only during peak solar radiation periods. This behavior reflects the continuous improvement in heat-transfer performance provided by the corrugated geometry. The larger effective absorber area enables more solar energy to be transferred to the basin water over the entire operating period, leading to sustained enhancement in evaporation and condensation rates. Consequently, the cumulative productivity increased from 2.97 kg/m²·day to 3.90 kg/m²·day, corresponding to an enhancement of approximately 31.12%.

The productivity enhancement can be attributed to the combined influence of increased heat-transfer area, higher basin-water temperatures, improved convective and evaporative heat-transfer coefficients, and stronger evaporation-condensation driving forces within the solar still. These findings demonstrate that basin geometry plays a significant role in determining the thermal and productivity performance of solar desalination systems. The obtained enhancement is consistent with previously reported studies on corrugated absorbers. Omara et al. [6], Ghandourah et al. [7], Sharshir et al. [8], and Kabeel et al. [10] reported noticeable productivity improvements when corrugated geometries were employed, confirming the positive influence of basin corrugation on solar still performance.

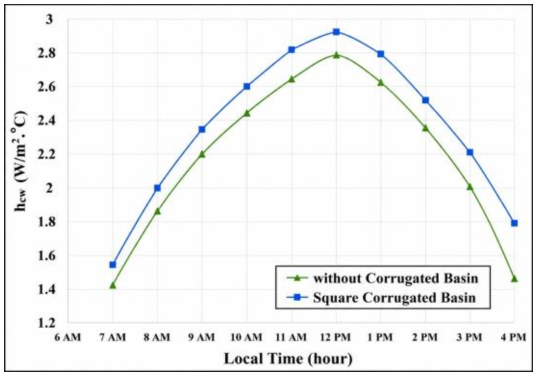

Figure 11. Comparison of convective heat transfer coefficient between conventional and square corrugated basins

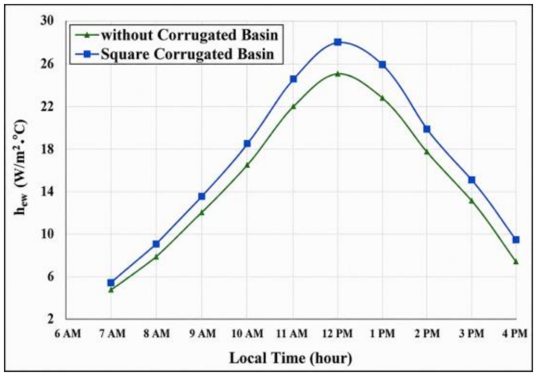

Figure 12. Comparison of evaporative heat transfer coefficient between conventional and square corrugated basins

Figure 15 presents the hourly thermal efficiency of the two solar still configurations. The square-corrugated basin exhibited higher thermal efficiency throughout the operating period because a larger fraction of the absorbed solar energy was effectively utilized in the evaporation process. The enhanced heat transfer from the basin surface to the water increased the conversion of solar energy into latent heat of vaporization rather than being dissipated through thermal losses. As a result, the average thermal efficiency increased from approximately 44.7% for the conventional basin to 67.3% for the square-corrugated basin. The thermal efficiency exceeded 100% during the final operating hours because the efficiency was calculated on an hourly basis. During this period, solar irradiance decreased sharply, whereas evaporation and condensation continued due to the thermal energy previously stored in the basin material and water mass. Consequently, the latent heat associated with the freshwater production temporarily exceeded the instantaneous solar energy input, leading to apparent efficiencies greater than 100%. This behavior is commonly observed in transient solar desalination systems and reflects the influence of thermal storage rather than a violation of energy conservation principles.

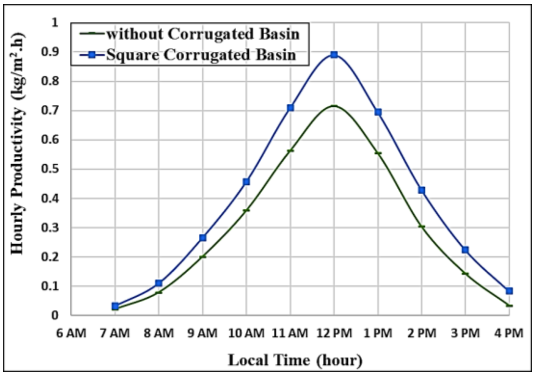

Figure 13. Numerical hourly productivity variation for the conventional basin and the square corrugated basin of the solar still

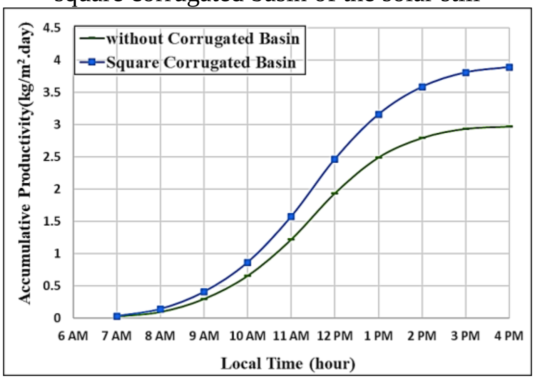

Figure 14. Numerical cumulative productivity variation for the conventional basin and the square corrugated basin of solar still

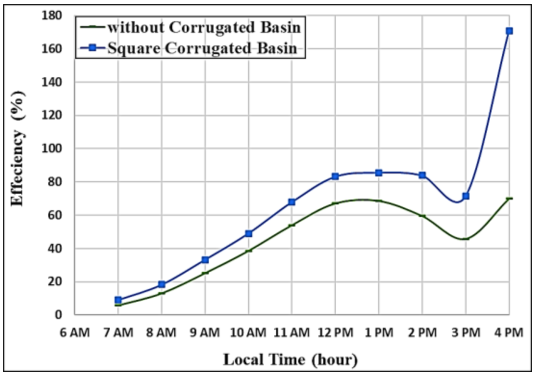

Figure 15. Thermal efficiency between the conventional basin and the square corrugated basin of solar still

4. Conclusion

The main conclusions of this study can be summarized as follows:

- A two-dimensional CFD model was developed to compare the thermal and productivity performances of conventional and square-corrugated basin solar stills under Basra climatic conditions.
- The square-corrugated basin increased the effective heat-transfer area, resulting in higher basin-water temperatures and improved thermal interaction between the absorber surface and the water layer.
- The enhanced geometry increased the convective and evaporative heat-transfer coefficients, thereby promoting stronger evaporation and condensation processes inside the solar still.
- The maximum hourly productivity increased from 0.72 kg/m²·h to 0.89 kg/m²·h, demonstrating the positive influence of basin corrugation on freshwater production.
- The cumulative productivity increased from 2.97 kg/m²·day to 3.90 kg/m²·day, corresponding to a productivity enhancement of approximately 31.12%.
- The average thermal efficiency improved from 44.7% for the conventional basin to 67.3% for the square-corrugated basin, indicating a more effective utilization of solar energy.
- The productivity enhancement was mainly attributed to higher basin-water temperatures,

improved heat-transfer coefficients, and stronger evaporation–condensation driving forces.

- The results confirm that square-corrugated basin geometry is a simple and effective modification for improving solar still performance without increasing the projected basin area or water mass.
- Future work should focus on experimental validation, economic feasibility assessment, and comparison with other corrugated basin geometries.

5. Study Limitations and Further Work

Although the square-corrugated basin showed clear performance improvement, the present study has some limitations. The numerical model focused mainly on heat transfer and did not directly simulate mass transfer, while the climatic input data were limited to a single day in Basra. In addition, simplifying assumptions such as constant projected basin area and basin-water mass were adopted. Future work should include direct mass-transfer modelling, longer-term and seasonal analyses, and further investigation of alternative basin geometries and key thermal parameters.

Acknowledgment

This work was partially supported by Southern Technical University under scientific research awards, No. 9/7934, 10 Sept. 2025.

Nomenclature

Symbol	Description	Unit
A_{square}	Effective area of a single square corrugation	m²
A_{total}	Total effective area of the corrugated basin	m²
CFD	Computational Fluid Dynamics	-
DO	Discrete Ordinates	-
E	Total energy per unit mass	J/kg
ER	Enhancement ratio	%
FVM	Finite Volume Method	-
g	Gravitational acceleration	m/s²
h	Corrugation height (depth)	mm
h_{cw}	Convective heat-transfer coefficient from water to glass cover	W/m²·K
h_{ew}	Evaporative heat-transfer coefficient from water to glass cover	W/m²·K
h_j	Enthalpy of species j	J/kg
I	Measured solar irradiance	W/m²
I_θ	Inclination-corrected solar irradiance	W/m²
J_j	Diffusion flux of species j	kg/m²·s
k_{eff}	Effective thermal conductivity	W/m·K
m_{ew}	Hourly freshwater productivity	kg/m²·h
N	Number of corrugations	–
P	Static pressure	Pa
p_h	Horizontal pitch of corrugation	mm
RMSE	Root Mean Square Error	-
S_h	Volumetric heat source term	W/m³
S_m	Mass source term	kg/m³·s
Ta	Ambient air temperature	°C
Tg	Glass-cover temperature	°C
Tw	Basin-water temperature	°C
u	Fluid velocity	m/s
VOF	Volume of Fluid	-
x_{mod}	Parameter value for modified basin	–
x_{ref}	Parameter value for conventional basin	–
ρ	Fluid density	kg/m³
τ	Stress tensor	N/m²
η	Thermal efficiency	%

References

1. Kannan, N. and D. Vakeesan. Solar energy for future world: - A review. Renewable and

Sustainable Energy Reviews. 2016;62(1092–1105. doi: 10.1016/j.rser.2016.05.022

2. Kaushal, A. and Varun. Solar stills: A review. Renewable and Sustainable Energy Reviews. 2010;14(1):446–453. doi: doi:10.1016/j.rser.2009.05.011
3. Kumar, P.V., et al. Solar stills system design: A review. Renewable and sustainable energy reviews. 2015;51(153–181. doi: http://dx.doi.org/10.1016/j.rser.2015.04.103
4. Manchanda, H. and M. Kumar. A comprehensive decade review and analysis on designs and performance parameters of passive solar still. Renewables: Wind, Water, and Solar. 2015;2(1):doi: DOI 10.1186/s40807-015-0019-8
5. Sivakumar, V. and E.G. Sundaram. Improvement techniques of solar still efficiency: A review. Renewable and Sustainable Energy Reviews. 2013;28(246–264. doi:
6. Omara, Z.M., et al. Experimental investigation of corrugated absorber solar still with wick and reflectors. Desalination. 2016;381(111–116. doi: https://doi.org/10.1016/j.desal.2015.12.001
7. Ghandourah, E., et al. Performance enhancement and economic analysis of pyramid solar still with corrugated absorber plate and conventional solar still: A case study. Case Studies in Thermal Engineering. 2022;35(101966. doi: https://doi.org/10.1016/j.csite.2022.101966
8. Sharshir, S.W., M.R. Elkadeem, and A. Meng. Performance enhancement of pyramid solar distiller using nanofluid integrated with v-corrugated absorber and wick: An experimental study. Applied Thermal Engineering. 2020;168(114848. doi: https://doi.org/10.1016/j.applthermaleng.2019.114848
9. Kabeel, A.E., et al. The impact of the corrugated absorber shape on the performance of a hemispherical solar still for water desalination: an experimental study. Applied Water Science. 2023;13(4):doi: https://doi.org/10.1007/s13201-023-01907-4
10. Kabeel, A., et al. Performance improvement of a tubular solar still using V-corrugated absorber with wick materials: Numerical and experimental investigations. Solar Energy. 2021;217(187–199. doi: https://doi.org/10.1016/j.solener.2021.02.008
11. Prasad, A.R., et al. Performance analysis of tubular solar still with different water depths on corrugated and flat absorbers. Journal of Water Supply: Research and Technology-Aqua. 2022;71(12):1425–1439. doi: doi: 10.2166/aqua.2022.253
12. Elshamy, S.M. and E.M.S. El-Said. Comparative study based on thermal, exergetic and economic analyses of a tubular solar still with semi-circular corrugated absorber. Journal of Cleaner Production. 2018;195(328–339. doi: 10.1016/j.jclepro.2018.05.243
13. Abdelaziz, G.B., et al. Performance enhancement of tubular solar still using nano-enhanced energy storage material integrated with v-corrugated aluminum basin, wick, and nanofluid. Journal of Energy Storage. 2021;41(doi: https://doi.org/10.1016/j.est.2021.102933
14. Hafs, H., et al. Numerical simulation of the performance of passive and active solar still with corrugated absorber surface as heat storage medium for sustainable solar desalination technology. Groundwater for Sustainable Development. 2021;14(doi: https://doi.org/10.1016/j.gsd.2021.100610
15. Abu-Zeid, M.A.-R., et al. Performance Enhancement of Solar Still Unit Using v-Corrugated Basin, Internal Reflecting Mirror, Flat-Plate Solar Collector and Nanofluids. Sustainability. 2024;16(2):doi: https://doi.org/10.3390/su16020655
16. Shalaby, S.M., E. El-Bialy, and A.A. El-Sebaii. An experimental investigation of a v-corrugated absorber single-basin solar still using PCM. Desalination. 2016;398(247–255. doi: http://dx.doi.org/10.1016/j.desal.2016.07.042
17. Jodah, F.T., et al. Experimental study of the performance of spherical solar stills using flat and corrugated circular absorbers with different techniques. Energy Sources, Part A: Recovery, Utilization, and Environmental Effects. 2025;47(2):doi: https://doi.org/10.1080/15567036.2025.2589922

18. Kabeel, A.E., et al. Performance enhancement of a v-corrugated basin hemispherical solar distiller combined with reversed solar collector: An experimental approach. Renewable Energy. 2022;190(330–337. doi: https://doi.org/10.1016/j.renene.2022.03.107
19. Essa, F.A., et al. Experimental multifaceted approach for enhance pyramidal solar still productivity: Tracking, corrugated absorber, reflectors, external condenser, and phase change material integration. Process Safety and Environmental Protection. 2025;197(doi: https://doi.org/10.1016/j.psep.2025.107061
20. Sharshir, S.W., et al. Thermo-economic performance improvement of hemispherical solar still using wick material with V-corrugated basin and two different energy storage materials. Solar Energy. 2023;249(336–352. doi: https://doi.org/10.1016/j.solener.2022.11.038
21. Dumka, P., et al. An Experimental Study on the Performance Enhancement of Solar Still Augmented with a Solar Fountain. Engineered Science. 2026;41(2201. doi: 10.30919/es2201
22. Kumar, R., D.R. Mishra, and P. Dumka. Comparative and experimental analysis of conventional solar still (CSS) and CSS augmented with a blend of peat and perlite. Desalination and Water Treatment. 2026;325(101713. doi: https://doi.org/10.1016/j.dwt.2026.101713
23. Dumka, P., et al. Enhancing distillate output in conventional solar stills through gel ball. Desalination and Water Treatment. 2025;323(101336. doi: https://doi.org/10.1016/j.dwt.2025.101336
24. Dumka, P., et al. Enhancing solar water desalination with wax infused glass for sustained distillate yield. Desalination and Water Treatment. 2025;322(101137. doi: https://doi.org/10.1016/j.dwt.2025.101137
25. Dumka, P., N. Pandey, and D.R. Mishra. Conventional Solar Still Augmented with Saltwater Bottles: An Experimental Study. Journal of Solar Energy Research. 2024;9(1):1811–1821. doi: 10.22059/jser.2024.374131.1392
26. Chauhan, R., S. Sharma, and R. Pachauri. Performance Prediction of Conventional and Modified Solar Stills Using Levenberg Marquardt Algorithm-Based Artificial Neural Network Model: An Experimental and Stochastic Evaluation. Journal of Solar Energy Research. 2024;9(3):1966–1980. doi: 10.22059/jser.2024.380006.1449
27. Bejan, A., <*Adrian_Bejanauth_Convection_Heat_Transfer,_Fourth_Edition_2013.pdf*>. 2013.
28. G.N. Tiwari , L.S. Advanced Solar-Distillation Systems: basic principles, thermal modeling, and its application. Green Energy and Technology. 2017;doi:
29. Dwivedi, V.K. and G.N. Tiwari. Comparison of internal heat transfer coefficients in passive solar stills by different thermal models: An experimental validation. Desalination. 2009;246(1):304–318. doi: https://doi.org/10.1016/j.desal.2008.06.024